Decay of Spatially Periodic Patterns in a Nematic Liquid Crystal

Nándor Éber,* Stanislaw A. Rozanski,† Szilárd Németh, and Ágnes Buka
Research Institute for Solid State Physics and Optics,
Hungarian Academy of Sciences, H-1525 Budapest, P.O.B.49, Hungary

Werner Pesch and Lorenz Kramer
Institute of Physics, University of Bayreuth, D-95440 Bayreuth, Germany
(Dated: August 30, 2004)

A detailed theoretical and experimental analysis of the decay of electroconvection patterns is presented in a planarly aligned nematic liquid crystal. The relaxation time is measured as a function of the wavenumber of the pattern using a light diffraction technique. A theoretical analysis exhibits a rich structure of the dispersion curves for the decay rates. An interesting relation between the realistic case of no-slip boundary conditions and the simpler free-slip case is found. The experimentally determined relaxation rates for both 'conductive' and 'dielectric' initial patterns follow the theoretical solution with subsequent jumps between branches when the wavenumber is increased.

PACS numbers: 47.54.+r, 61.30.Gd, 61.30.Dk, 42.25.Fx, 78.20.Jq

I. INTRODUCTION

Systems far from equilibrium often respond to excitations by creating spatially periodic patterns. Anisotropic fluids - like nematic liquid crystals - are especially rich in pattern forming phenomena [1]. The mean orientation of the elongated nematic molecules or equivalently the local optical axis is described by the director $\mathbf{n}$ with $\mathbf{n}^2 = 1$. Electroconvection (EC) driven by an AC voltage applied across a thin (thickness $d \sim 10 - 100\mu$m) nematic layer is a common example of pattern forming instabilities [2]. EC is a threshold phenomenon which usually occurs as a primary instability in a slightly conducting nematic with negative dielectric and positive conductivity anisotropies (or vice versa [3, 4]). The pattern then appears at onset in the form of a periodic array of parallel convection rolls (wave number q) coupled to a periodic modulation of the director orientation, which results in a sequence of dark and bright stripes observable in a microscope. Varying the easily tunable control parameters like the AC-voltage (rms amplitude V, frequency f), magnetic field, temperature, etc. a wide variety of scenarios can be generated which makes electroconvection a popular model system for pattern formation studies. In particular the characteristic wavenumber q of the patterns depends sensitively on f.

When the excitation is turned off the roll pattern decays as the system returns to its equilibrium (usually homogeneous) state. Though the relaxation time τ characterizing this decay process gives important insight into the nemato-hydrodynamic mechanism, it has so far not been analyzed systematically. It will be demonstrated in this paper, where we focus in particular on the dependence of τ on q that such an analysis gives interesting new insights.

The various mechanisms responsible for EC are active on different characteristic time scales. The slowest time scale is given by the director relaxation time $\tau_d = \frac{\gamma_1 d^2}{K_{11}\pi^2}$, which sets the time scale for director reorientations, where γ_1 denotes the rotational viscosity, and K_{11} is the splay elastic modulus. The charge relaxation time $\tau_q = \frac{\epsilon_0 \epsilon_\perp}{\sigma_\perp}$ is considerably shorter than τ_d ($\epsilon_\perp$ is the dielectric permittivity and $\sigma_\perp$ the conductivity component perpendicular to the director). The viscous relaxation time $\tau_{visc} = d^2/\nu$ characterizing the viscous damping (ν is the kinematic viscosity) of flow is much shorter than the other time scales, so the velocity field can be treated adiabatically. In some situations (not considered here), when one is for instance in (or near to) the regime where traveling waves appear at onset, the treatment of a nematic as an ohmic conductor is insufficient. Then an additional time scale related to the recombination of charge carriers τ_{rec} becomes relevant (WEM-model [5]).

Ideally all of the above processes contribute to the decay time, making the process very complex. Fortunately the fast processes (charge relaxation and the viscous damping) contribute only at the very beginning of the decay process, whereas the only relevant time scale at the later stage of the relaxation process is expected to be τ_d. Thus, the process is expected to be rather universal, independent of the excitation mechanism. In fact, the only relevant quantity determining the long-time decay should be the wave number q, which (ideally) remains unaltered during the decay. Comparing the theoretical predictions with experiments could even be used to determine material parameters such as the viscosity (Leslie) coefficients.

The theoretical task of determining the asymptotic decay times of a pattern with nonzero wave number is in principle straightforward and conceptionally less complicated than the problem of EC, since only the director deformation and the flow field (back flow) are involved.

*Electronic address: eber@szfki.hu
†on leave from Higher Vocational State School in Pila, ul. Podchorazych 10, PL-64920 Pila, Poland

In addition the pattern amplitudes continuously decrease when the decay process advances, thus the analysis can be based on the linearized nemato-hydrodynamic equations. Nevertheless so far the problem has been treated in the literature only in a 'single mode' approximation (SMA) where the boundary conditions for the velocities are not implemented properly [6, 7].

Experimental studies of EC patterns are most often based on recording and digital processing of (stationary) shadowgraph images in a polarizing microscope. In the present experiment we have to resolve fast decay of low contrast (small deformations) patterns. The standard 25 Hz (or slower) video rate of common analog and/or digital cameras impose a strong constraint on the recording speed and the typical 8 bit video digitization may also not provide sufficient gray-scale resolution. The shadowgraph technique is therefore less appropriate for the analysis of the decay process unless special instrumentation is used.

On the other hand EC patterns represent a periodic optical grating. Illuminating them with a monochromatic (laser) light beam results in a diffraction pattern. The intensity I_n of the nth order fringe is for not too large pattern amplitude ϑ_m given by

$$I_n = B_n \Big[J_n(Q\vartheta_m) \Big]^2, \qquad (1)$$

where J_n is the Bessel-function of first kind of order n, while the quantities B_n and Q depend on the refractive indices, the angle of incidence and the shape of the director profile[11, 12]. In the limit of small ϑ_m, which is relevant for our study, we have $I_n \propto \vartheta_m^{2n}$. Thus the I_n for small n prevail. For symmetry reasons only the even order fringes are visible (at least for small deformations) at normal light incidence [8–11]. For oblique incidence [11, 12], however, the odd order fringes (in particular $n = 1$) become accessible, which thus present a sensitive tool to monitor variations of EC pattern amplitudes near the threshold.

Based on these considerations an interesting optical method has recently been proposed to measure the relaxation times τ by diffraction on EC patterns [7]. The initial roll pattern has been induced by periodically switching the DC voltage between positive, zero and negative values. The intensities of low-order fringes have been recorded, which have shown a sawtooth-like modulation due to the periodic reorientation of the director (growth and decay of the pattern) and the relaxation time has been obtained by fitting to results of the SMA approach. The method has only been applied to a single switching frequency of the excitation where τ is claimed to match the theoretical value. The analysis would have been more convincing, if by varying the switching frequency the wavenumber q of the EC pattern (which is a crucial parameter for τ) had been systematically changed.

The approach in Ref. [7] has some disadvantages. Firstly, it captures only the beginning of the decay process where one cannot expect a single time-exponent to govern the dynamics. Furthermore, the theoretical analysis makes use of the SMA, which, although quite effective for the description of the EC state near threshold, is questionable for the relaxation process.

The work presented in this paper has two aims. On the one hand the experimental technique was improved, using sine wave AC voltage excitation that allowed to measure the wavelength dependence of the relaxation times in a wide q range. Moreover we focused on the late stage of the relaxation process, which should be determined by a single relaxation time. On the other hand we present a rigorous theoretical analysis of the relaxation time problem with proper handling of the boundary conditions. The results given in Section II reveal some surprising features.

We want to stress again that though the pattern was created by electroconvection, the relaxation occurred in the absence of electric field. Thus the results obtained are valid for the decay of any other patterns which are characterized by periodic splay-bend deformation of the director (e.g. shear flow induced convection rolls).

II. THEORY OF THE DECAY

The system under study is a nematic layer of thickness d confined by plates parallel to the $x-y$ plane. We assume strong planar anchoring of the director at the bounding plates in the x direction, so in the rest (i.e. basic) state the director ($\mathbf{n} = (n_x, n_y, n_z)$) is given as $\mathbf{n} = (1, 0, 0)$. We consider a situation where a spatially periodic pattern with wavevector $\mathbf{q} = (q, p)$ in the $x-y$ plane has been generated, e.g. by electroconvection. We will discuss in general terms the relaxation process after switching off the excitation. One is then left with the standard nematodynamic equations for the Cartesian components of the director field $\mathbf{n}$ and of the velocity field $\mathbf{v} = (v_x, v_y, v_z)$, see e.g. [13–15]. We will use dimensionless units. The unit of length is chosen to be d/π, time is measured in units of the director relaxation time τ_d, elastic moduli are scaled with the splay elastic constant K_{11}, viscosity coefficients by the rotational viscosity γ_1.

Here, we restrict ourselves to normal roll patterns with $p = 0$ (no y dependence). Thus all fields depend only on x and z. The y components of $\mathbf{n}$ and $\mathbf{v}$ vanish. In the nematodynamic equations linearized about the basic state, which are sufficient for the late stage of the decay process the dependence on x becomes harmonic, e.g $n_z(x, z, t) = \bar{n}_z(z, q, t) sin(qx), v_z(x, z, t) = \bar{v}_z(x, q, t) cos(qx)$. Since the decay process is slow compared to the viscous relaxation time τ_{visc}, time derivatives of $\mathbf{v}$ can be (adiabatically) neglected. After eliminating v_x with the help of the incompressibility condition $\nabla \cdot \mathbf{v} = 0$ we arrive at the following linear equations:

$$\begin{aligned} \big[\partial_t + K_{33}q^2 \; - \; \partial_z^2\big] q\bar{n}_z(z,q,t) \\ - \; [\alpha_2 q^2 + \alpha_3 \partial_z^2] \bar{v}_z(z,q,t) = 0, \end{aligned} \qquad (2)$$

$$[\alpha_2 q^2 + \alpha_3 \partial_z^2] q \partial_t \bar{n}_z(z,q,t) - [\eta_2 \partial_z^4 - \eta_r q^2 \partial_z^2 + \eta_1 q^4] \bar{v}_z(z,q,t) = 0, \quad (3)$$

where

$$\eta_1 = (-\alpha_2 + \alpha_4 + \alpha_5)/2\ ; \quad \eta_2 = (\alpha_3 + \alpha_4 + \alpha_6)/2\ ; \quad \eta_r = \eta_1 + \eta_2 + \alpha_1 \quad (4)$$

are effective (Miesowicz) shear viscosities. Note that the correction to $n_x = 1$ (basic state) vanishes at linear order. In the following the bars in $\bar{n}_z$ and $\bar{v}_z$ will be suppressed for simplicity.

These equations have to be supplemented with realistic rigid boundary conditions, i.e. strong planar anchoring of the director and no slip for the velocities at the bounding plates at $z = \pm\pi/2$ in dimensionless units:

$$n_z = 0, \quad v_z = 0, \quad \partial_z v_z = 0 \qquad \text{at} \qquad z = \pm\pi/2. \quad (5)$$

The last condition follows from $v_x(\pm\pi/2) = 0$ and $\nabla \cdot \mathbf{v} = 0$.

The velocity component v_z can be eliminated yielding a partial differential equation for the director component $n_z(z,q,t)$

$$\left[(\alpha_2 q^2 + \alpha_3 \partial_z^2)^2 - (\eta_2 \partial_z^4 - \eta_r q^2 \partial_z^2 + \eta_1 q^4)\right] q \partial_t n_z(z,q,t) - \left[\eta_2 \partial_z^4 - \eta_r q^2 \partial_z^2 + \eta_1 q^4\right](K_{33} q^2 - \partial_z^2) q n_z(z,q,t) = 0. \quad (6)$$

Equation (6) allows modal solutions in exponential form $n_z(z,q,t) = n(s,q) e^{-\mu t} e^{isz}$ (analogously one has $v_z(z,q,t) = v(s,q) e^{-\mu t} e^{isz}$). Thus we arrive from Eq. (6) at the following dispersion relation:

$$(\alpha_2 q^2 - \alpha_3 s^2)^2 \mu + (\eta_2 s^4 + \eta_r q^2 s^2 + \eta_1 q^4)(K_{33} q^2 + s^2 - \mu) = 0. \quad (7)$$

Clearly Eq. (7) involves only two independent variables s^2/q^2 and μ/q^2. Obviously one can superpose modes with s and $-s$ to yield real solutions with a given parity (reflection symmetry in z). From Eq. (2) we see that the amplitudes $n(s,q)$ and $v(s,q)$ of the modal solutions are related by

$$n(s,q) = G(s,q) v(s,q) \quad (8)$$

with

$$G(s,q) = \frac{\alpha_2 q^2 - \alpha_3 s^2}{q(K_{33} q^2 + s^2 - \mu)}. \quad (9)$$

In a rigorous treatment one has to take into account that Eq. (7) is a cubic equation in s^2, which provides three roots (s_1^2, s_2^2 and s_3^2) for each μ and q which are to be superposed to satisfy the realistic no-slip boundary conditions. We expect that only situations where n_z and v_z are even functions of z will be of relevance. Thus, the exact solution of the decay problem is a linear combination of cosine functions constructed from the roots of Eq. (7),

$$n_z(z,t) = e^{-\mu t} N(z) = e^{-\mu t} \Sigma_{j=1}^3 A_j G_j \cos(s_j z)$$
$$v_z(z,t) = e^{-\mu t} V(z) = e^{-\mu t} \Sigma_{j=1}^3 A_j \cos(s_j z) \quad (10)$$

with $G_i = G(s_i, q)$ calculated from Eqs. (8),(9). Combining Eq. (5) with Eq. (10) a set of 3 homogeneous linear equations are obtained for the weights A_1, A_2 and A_3. A non-trivial solution exists if the corresponding determinant vanishes. Thus one obtains a discrete eigenvalue spectrum $\mu_k(q^2)$, $k = 1, 2, \ldots$ with the corresponding eigenfunctions $N_k(z)$ and $V_k(z)$ (see Eqs. (10)). As to be expected the μ_k are found to be real and positive. We will order them in increasing magnitude ($\mu_1 < \mu_2 < \ldots$) in the following.

Before we discuss the resulting eigenvalue spectrum in detail, which requires numerical calculations, we will address the situation in the SMA approximation. This case is obtained by replacing the last condition in Eq. (5) by $\partial_z^2 v_z = 0$, which corresponds to the unrealistic case of zero tangential stress on the velocity field ("free slip"). Then the even eigenfunctions $N_k(z), V_k(z)$ are proportional to $\cos(S_k z)$ with $S_k = 2k - 1$, $k = 1, 2, 3, \ldots$, independent of q^2. Thus the s in the dispersion relation can be identified with S_k and for the free-slip eigenvalues $\bar{\mu}_k(q^2)$ one obtains

$$\bar{\mu}_k = \frac{\hat{\mu}_k}{1 - b_k}, \qquad \text{with} \qquad \hat{\mu}_k = S_k^2 + K_{33} q^2,$$
$$b_k = \frac{(\alpha_2 q^2 - \alpha_3)^2 S_k^2}{\eta_2 S_k^4 + \eta_r q^2 S_k^2 + \eta_1 q^4}. \quad (11)$$

Note that $\bar{\mu}_1$ coincides with the growth rate (properly nondimensionalized) on which the analysis in Ref. [7] was based (see Eq. (7) there). Also note that $\hat{\mu}_k$ presents a set of purely elastic (no back flow) decay rates. Thus $\hat{\mu}_1$ gives the slowest decay mode in this limit of vanishing viscosities. The (positive) quantities b_k describe the enhancement of the decay by back flow. Whereas $\hat{\mu}_1$ should underestimate the actual decay constant, $\bar{\mu}_1$ is expected to give a bound from above, since the free-slip boundary conditions are less restrictive than the rigid ones to the flow field.

A surprising feature appears when the higher branches $\bar{\mu}_k$ of the SMA are considered. Figure 1a displays the 10 first branches ($\bar{\mu}_1, \ldots, \bar{\mu}_{10}$) as a function of q^2 for the parameter set of Phase 5/5A listed in Table I. One sees that the "natural" ordering $\bar{\mu}_1 < \bar{\mu}_2 < \bar{\mu}_3 < \ldots$ applies only for small q^2. With increasing q^2 the higher-indexed branches $\bar{\mu}_k(q^2)$ cross all the lower-indexed ones. Thus, each branch becomes the lowest within some interval of q^2. The explanation for this behavior is that for the slowest mode the spatial variation along x, characterized by q, are balanced by a corresponding variation along z, characterized by S_k. Clearly there exists an envelope, which bounds all SMA branches from below. For large q^2 the envelope becomes a straight line through the origin whose slope is determined by the minimum of $\bar{\mu}_k/q^2$ for large q^2 minimized over k. This minimum is obtained by treating S_k as a continuous variable and minimizing $\bar{\mu}_k$, which gives $Min(\bar{\mu}_k/q^2) = \Xi = 4.2285$ at $S_k^2 = 1.0493 q^2$ for our material parameters.

Returning to the rigorous eigenvalue spectrum $\mu_k(q^2)$, Figure 1b displays the lowest 10 branches ($\mu_1, \ldots, \mu_{10}$)

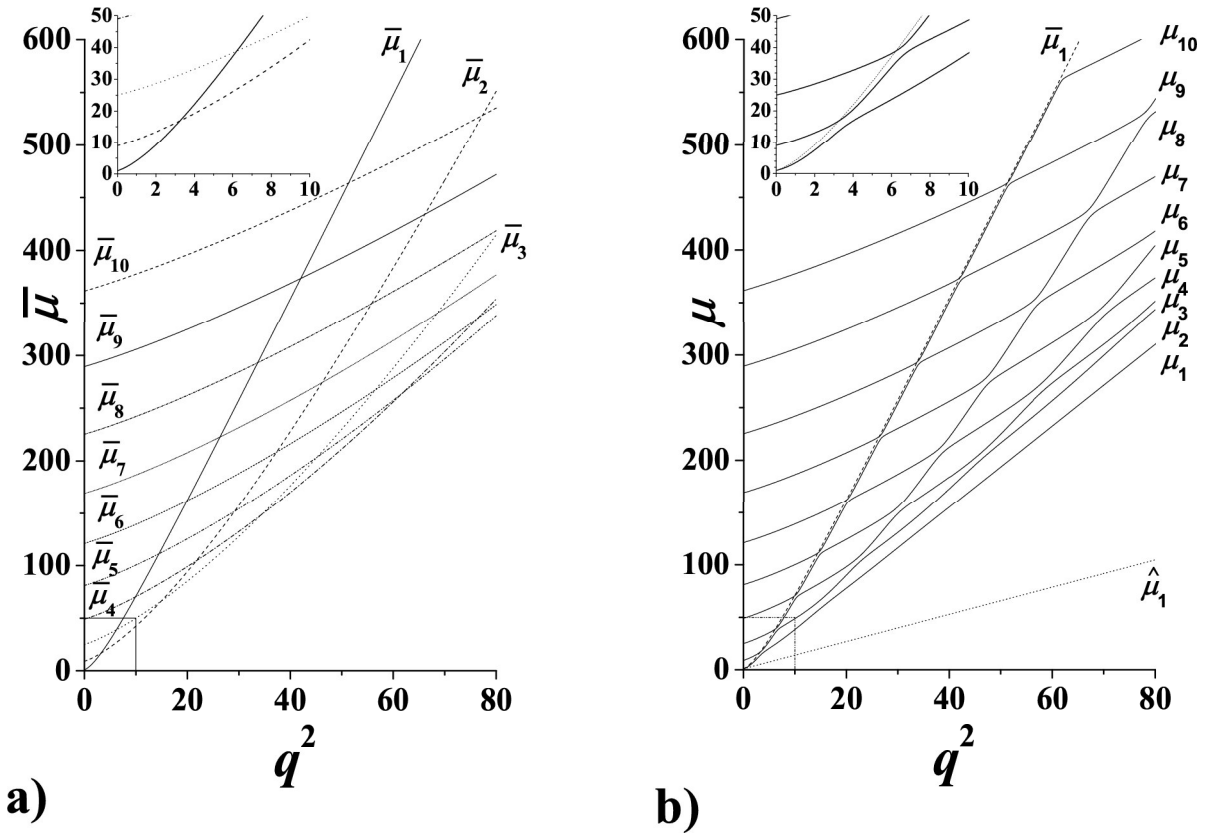

FIG. 1: Theoretical values of the dimensionless decay rate of the director distortion versus dimensionless q^2 calculated for the parameter set of Phase 5/5A. a) The 10 lowest $\bar{\mu}_k$ branches of the dispersion relation for the case of free-slip boundaries. b) Solid lines show the 10 lowest μ_k branches of the dispersion relation obtained from the rigorous calculation. Dashed and dotted lines correspond to the SMA branch $\bar{\mu}_1$ and to the flow free case ($\hat{\mu}_1$), respectively. The inserts show the corresponding lowest 3 branches enlarged for low q^2.

TABLE I: The material parameters of the nematic Phase 5/5A used for the numerical calculations.

Quantity	Unit	Value at 30°C	Reference
K_{11}	10^{-12}N	9.8	[16]
K_{33}	"	12.7	"
α_1	10^{-3}Ns/m^2	-39	[16]
α_2	"	-109.3	[16, 17]
α_3	"	1.5	"
α_4	"	56.3	"
α_6	"	-24.9	"

as a function of q^2 (solid lines, parameter set of Phase 5/5A). The decay rates $\bar{\mu}_1$ (SMA) and $\hat{\mu}_1$ (no back flow) are also shown (dashed and dotted lines respectively). The rigorous solution offers modes with smaller eigenvalues μ_k (longer decay) than $\bar{\mu}_1$. In fact the lowest branch $\mu_1(q^2)$ remains below $\bar{\mu}_1(q^2)$ for any q^2, see also the inset (actually, $\mu_1(q^2)$ remains below all $\bar{\mu}_k(q^2)$, see below). As expected, $\hat{\mu}_1$ gives a lower bound. For $k > 1$, each μ_k branch crosses $\bar{\mu}_1$ at some q^2 and in that neighborhood the slope increases and approaches that of $\bar{\mu}_1$, so that the two curves remain close to each other (with $\bar{\mu}_1 > \mu_k$) in some q^2 interval. For $k = 2, 3, \ldots$ these intervals follow each other and build up an almost continuous line running just below $\bar{\mu}_1$ (for large k the effect becomes more pronounced).

More generally, the branches $\mu_k(q^2)$ consist of alternate pieces with higher and lower slopes forming a step-like curve. The branches do not touch or cross each other. One notices a close similarity with the structure of the SMA curves in Figure 1a. There, however, the curves cross each other. Substantial deviations occur only in the vicinity of the crossing points of the branches $\bar{\mu}_k(q^2)$. In fact, it is quite common in physics that a dispersion relation is composed of crossing branches in some "unperturbed" approximation while the rigorous solution of the same problem results in combination of the branches and gap formation at the crossing points (see e.g. the electronic band structure in crystals in the nearly-free electron limit). Here the unperturbed problem corresponds

to the free-slip case. Indeed, for $q^2 >> 1$, the influence of no-slip boundary conditions is in effect a small perturbation that becomes important near the points of degeneracy (the crossings) of the unperturbed eigenvalues.

It follows from Eq. (10) that the eigenmodes $N_k(z,q), V_k(z,q))$ are not simple harmonic functions of z. In Figure 2 the function $N_1(z)$ is shown for the lowest branch μ_1 at $q^2 = 1,\ 10$, and 100. At small q, where μ_1 is close to $\bar{\mu}_1$, one has $N_1(z) \sim cos(z)$. This changes drastically as q increases, where $N_1(z)$ eventually develops into a boundary layer (this is the case for $k = 1$ only, see below). In general we can identify an index k_0 associated with a certain q^2-interval where μ_{k_0} is close to $\bar{\mu}_1$. Within that interval the corresponding eigenmodes $N_{k_0}(z)$ are dominated by a contribution $\sim cos(z)$ superimposed with oscillations $\sim cos(2k_0 z)$ of small amplitude. To the left of those intervals the contribution $\sim cos(z)$ eventually vanishes and the eigenmodes are dominated by a fast oscillation $\sim cos[(2k_0 - 1)z]$. To the right of those intervals the $cos(z)$ contribution shifts towards $cos(3z)$ though with small amplitude superimposed with a strong $\sim cos[(2k_0+1)z]$. The profiles $N_{10}(z)$ shown in Fig. 3 for $q^2 = 58$ (inside the interval $k_0 = 10$), 40 (below interval) and 76 (above interval) demonstrate this effect. More generally, the eigenfunctions on the jth steep portion of the μ_k branches become approximately proportional to $cos((2j-1)z)$ with $j = 1, 2, \ldots$, while on the next flat portion a $cos((2(k+j)-1)z)$ dependence dominates. One may conclude that an exact eigenfunction $N_j(z,q)$ is similar to a SMA eigenfunction $cos(2k-1)z$ whenever the eigenvalue $\mu_j(q^2)$ is near to $\bar{\mu}_k(q^2)$.

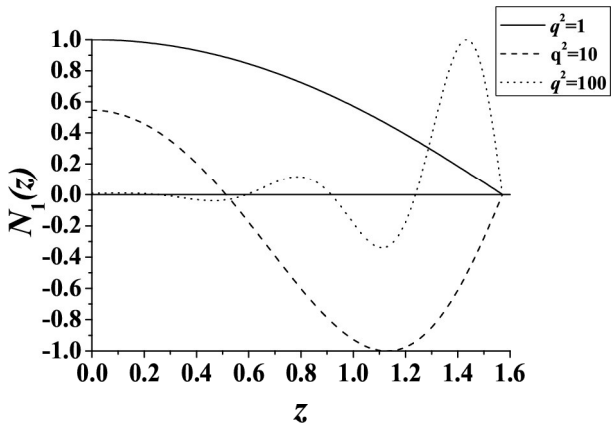

FIG. 2: Normalized director profile $N_1(z)$ belonging to the μ_1 mode calculated for the parameter set of Phase 5/5A at $q^2 = 1,\ 10$ and 100 respectively.

Interestingly, for not too small q^2, the lowest branch μ_1 remains separated from the rest (and separated from all SMA branches). This can be understood most easily by looking, in the limit $q^2 \to \infty$, at the quantity $Min(\bar{\mu}_k/q^2) = \Xi$ from another side. Ξ corresponds to the point where μ/q^2, as given in the dispersion relation

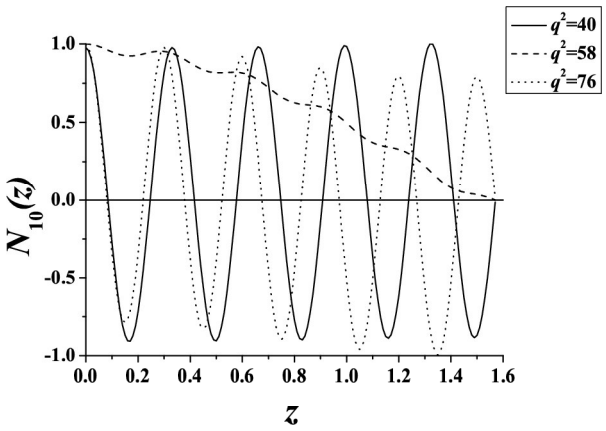

FIG. 3: Normalized director profile $N_{10}(z)$ belonging to the μ_{10} mode calculated for the parameter set of Phase 5/5A at $q^2 = 40,\ 58$ and 76 respectively.

Eq. (7) as a function of s^2, has a minimum, i.e. where two roots s_1^2 and s_2^2 of the dispersion relation coincide (note that the s_i^2 scale with q^2). Below this point ($\mu/q^2 < \Xi$) the dispersion relation has two complex conjugate roots s_1^2 and s_2^2 and a negative root s_3^2. Thus all s_1, s_2, and s_3 have (substantial) imaginary parts so that the e^{is_j} decay rapidly either to the left or to the right depending on the choice of sign. Then one can construct, at some value of μ ($= \mu_1 = 3.8801q^2$) a solution of the problem that decays away from either boundary and which represents a boundary layer solution. For $\mu/q^2 > \Xi$ the complex conjugate pair becomes real. Near Ξ their difference is small and their superposition describes a slowly modulated, rapidly oscillating function (the rapidly decaying contribution from s_3 remains localized near to the boundary). This gives the branches $\mu_2, \mu_3, \ldots$, which are characterized by an increasing number of modulation periods. In the limit of large q^2 they form a quasi continuum, well separated from μ_1.

The knowledge of the decay rates is not sufficient to describe the decay process fully. Firstly one needs the initial state before switching off the voltage, which involves solving the full linear (for small ϵ) EC problem as a function of frequency for the given nematic. This is numerically cumbersome, in particular in the 'dielectric' (large q) regime. The initial condition determines the expansion coefficients A_i (see Eq. (10)). Since the eigenvalue problem Eqs. (2), (3) is not self-adjoint one has to solve the adjoint problem as well. Finally the contribution of the different modes to the intensity of the fringes has to be calculated following e.g. the methods presented in [10, 11]. The corresponding detailed analysis is presently under way.

III. EXPERIMENTAL

In order to cover a large range of decay rates μ and/or wave numbers q^2, the decay of EC patterns was investigated in planar samples of the nematic mixture Phase 5 (Merck) and on its factory doped version Phase 5A. These substances are popular in the investigation of EC, since they are chemically stable and their material parameters are well characterized [16, 17].

Planar cells were assembled using rubbed polyimide coated electrode surfaces made by E.H.C. Co. The transparent ITO electrodes covered a surface of 1cm*1cm. The thickness d of the cells was adjusted by nylon spacers, and was determined by an Ocean Optics spectrophotometer before filling.

EC was driven by sinusoidal voltage synthesized by a function generator PC card through an electronic switch and a high voltage amplifier. This switch allowed an abrupt (within 10μs) shutting down of the applied voltage. The actual AC voltage across the sample was measured by a digital voltmeter.

The sample was thermostatted by a PC controlled Instec hot-stage at $T = 30.0 \pm 0.05$°C. A beam of a laser-diode of wavelength $\lambda = 650$nm illuminated the cell on an area of about 1mm * 2mm. In the state of electroconvection a highly regular diffraction pattern could be observed as a sequence of light spots on a screen placed normal to the beam at a distance of $L = 660$mm. As the hot stage could be rotated around an axis in the plane of the cell perpendicular to the director, diffraction at normal as well as at oblique incidence of light could be investigated. Depending on the applied voltage diffraction fringes up to the 9th order could be seen. At higher voltages, however, the diffraction spots gradually became diffuse indicating the reduction of pattern regularity (appearance of defects above the threshold for secondary instabilities) and finally faded into an almost uniformly scattering background (the turbulent, dynamic scattering mode).

The higher sensitivity of diffraction at oblique incidence could be clearly demonstrated by the fact that a couple of diffraction orders were still visible at low voltages where no fringes could be seen at normal incidence. Therefore the measurements shown were carried out at an angle of incidence $\beta = 5\,°$.

In EC one usually observes two types of patterns, 'conductive' and 'dielectric' rolls. In the first regime (at frequencies f below the cut-off frequency f_c) the director distortion is virtually stationary and the dimensionless q is of the order of one, while in the latter regime ($f > f_c$) n_z follows the external AC frequency and $q >> 1$ can easily be obtained. f_c is roughly proportional to the electric conductivity of the sample.

Using Phase 5A in a cell of $d = 28\mu$m thickness EC patterns of the 'conductive' type existed in a wide frequency range ($10 - 1380$Hz). For $f > 1200$Hz the threshold of the EC patterns grew steeply with the frequency. Thus the highest accessible frequency (which was still below the cut-off) was practically limited by the maximum sinusoidal output voltage ($\pm 160 V_{peak}$) the high-voltage amplifier could provide which was too low to enter into the 'dielectric' regime. Normal rolls, i.e. fringes along a single line parallel to the director appeared above the Lifshitz point f_L. At low frequencies ($f < f_L \approx 200$Hz) oblique rolls were observed which resulted in diffraction fringes aligned along two crossing lines as expected.

The wavelength of the pattern varied from $\Lambda = 47.4\mu$m at low f to $\Lambda = 16.6\mu$m at the highest $f = 1380$Hz. The dimensionless q^2 fell into the range $1.4 - 11.3$. At lower f the accuracy of q^2 was mainly determined by the precision of distance measurements on the screen, while at higher frequencies the increase of the fringe diameter was the main limiting factor.

In order to study the large q regime we investigated the decay of the 'dielectric' rolls in a thinner ($d = 9.2\mu$m) cell filled with Phase 5 having much lower electric conductivity. The 'dielectric' regime occurred above $f_c \simeq 100$Hz. The low frequency 'conductive' regime with oblique rolls occuring up to $f_L \simeq 60$Hz has not been examined in detail. The wavelength of the 'dielectric' rolls was substantially smaller than in the 'conductive' regime (as expected), and could be tuned from $\Lambda = 4.6\mu$m to $\Lambda = 2.9\mu$m by increasing the frequency. In dimensionless units a range from $q^2 = 14$ to $q^2 = 38$ has been covered. At these smaller Λ the diffraction angles were higher and thus fewer number of fringe orders were visible. In general the diameters of the diffraction spots corresponding to the 'dielectric' rolls were noticeably larger indicating less regular patterns. Note that the conductivities of the two samples and the thickness of the cells have been chosen in such a way that the (dimensionless) wavenumbers q in the two regimes joined almost continuously (see also Fig. 7.

In order to study the decay of electroconvection patterns the intensity of the diffracted light was monitored. An optical fibre (with a diameter of 1 mm) which was positioned at the centre of the selected fringe (typically the 1st order one) transmitted the diffracted light into a photomultiplier working in its linear regime. Its output was fed through a current-to-voltage converter into a 16-bit A/D converter card. That allowed recording of the intensity at high precision with adjustable sampling rate.

As already mentioned in the introduction, the light intensity I_n of an nth order fringe is proportional to $\vartheta_m(t)^{2n}$. Hence, assuming an exponential decay of the deformation ($\vartheta_m = \vartheta_0 e^{-t/\tau}$) the characteristic time for the intensity decay of the nth order fringe is given by $\tau_n^* = \tau/2n$. Thus higher order fringe intensities decay faster, moreover, their intensities ($\propto \vartheta_0^{2n}$) are smaller and more sensitive to nonlinear corrections. Consequently we concentrated the detailed analysis on I_1 which is accessible in the case of oblique incidence.

The wavelength Λ of the EC pattern can conveniently be tuned by the frequency f of the excitation. At each f first the EC threshold voltage V_c was determined based on visibility criteria. Then the voltage V was raised by 1

% which corresponds to a value of $\varepsilon = (V^2 - V_c^2)/V_c^2 = 0.02$ of the dimensionless control parameter. At this ε typically 4 diffraction orders were visible. Λ was then determined by measuring the distances D_n between the nth order diffraction fringes and the main beam (zeroth order) and using the condition for constructive interference

$$\Lambda(\sin\beta + \sin(\alpha_n - \beta)) = n\lambda, \qquad (12)$$

where β is the angle of incidence and $\alpha_n = \arctan(D_n/L)$ is the diffraction angle for the nth order fringe.

The detector was then positioned at the centre of the 1st order fringe (to the place of maximum intensity) to monitor temporal variations. Data acquisition was started at the instant of switching off the applied voltage. Figure 4 shows some examples of the decay curves obtained when starting from different ε values. Note that the fringe intensity is not expected to grow monotonically with ε (although ϑ_m does so), as the Bessel function in Eq. (1) is an oscillating function of its argument. The dotted curve in Fig. 4 indicates that at $\varepsilon = 0.066$ the deformation is already large enough to get past the first maximum of Eq. (1) which explains the slight increase of the intensity at the initial part of the decay.

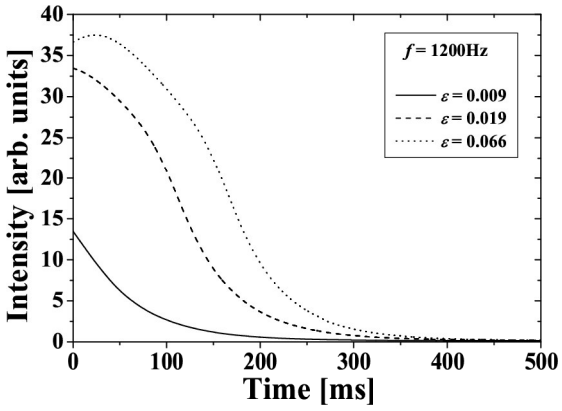

FIG. 4: Temporal evolution of the light intensity of the 1st order diffraction fringe I_1 following the shut-down of the applied voltage in a 28 μm thick cell of Phase 5A. Curves with different line styles correspond to different initial value of the dimensionless control parameter ε (which sets the pattern amplitude).

In order to focus onto small deformations, however, during measurements the gain of the A/D converter was increased by a factor of 8. Furthermore, we zoomed in on the tail (on values below 1/16 of full scale) of the relaxation curve. This tail section which showed an exponential decay was finally recorded as 3000 points with a 12 bit resolution. The sampling time was chosen so that the recorded section corresponded to a period of about $6 - 7\tau_1^*$. Before processing the data they were smoothed by a sliding averaging involving 51 neighboring data points. This improved the signal-to-noise ratio considerably while it did not affect the exponential shape of the curve. Finally the relaxation time of the fringe intensity, $\tau_1^* = \tau/2$, was obtained by a least square fitting of a single exponential. Figure 5 depicts an example of the recorded data and the fitted exponential. The mean square deviation of the experimental data from the fitted curve is typically less than 1 % of the full scale hence a systematic deviation is almost undetectable in the figure.

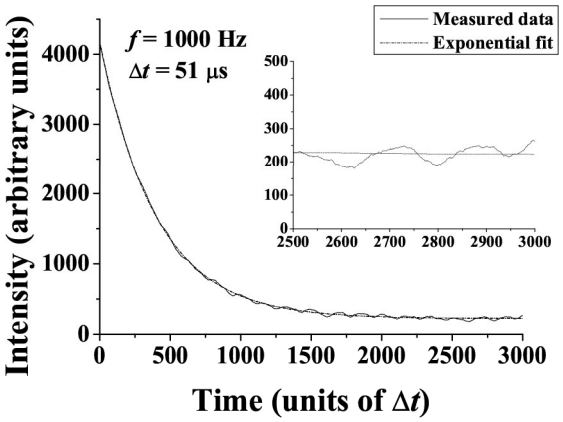

FIG. 5: The tail of the decay curve with a fitted exponential. The insert shows the final part in an enlarged form.

Despite of the good fit the relaxation times τ obtained from repeated recordings showed a typical scattering of about 10 %. Therefore the results were averaged for 10 consecutive measurements ($\bar{\tau}$) at the same frequency and finally the dimensionless decay rate was calculated by scaling with the director relaxation time ($\mu_{exp} = \frac{\tau_d}{\bar{\tau}}$).

The procedure above could not be fully applied to the thin cell in the 'dielectric' regime. As a consequence of the smaller wavelength of the 'dielectric' rolls (which is independent of d and is a combination of material parameters), their relaxation time turned out to be quite short (0.14−0.48ms) compared to the minimum sampling time (0.01ms) of the high resolution A/D converter card. Therefore in this case a digital oscilloscope with an 8-bit resolution was used to record the temporal evolution of the fringe intensity and all recorded points (except those saturating due to overdriving at the start of the decay) were included in the exponential fitting.

IV. COMPARISON OF EXPERIMENTAL DATA WITH THEORY

Figure 6 displays the measured data together with the theoretical curves in the conductive range. Focusing on the very end of the relaxation process we expected that there the system decays with the slowest rate μ_1 in the

whole q range because faster modes die out earlier. It can be seen, however, that the measured points do not follow the lowest branch of the dispersion relation (the slowest decaying mode) except in the very low q^2 range up to about 4. Neither do they follow the predictions of the SMA as all points are below that curve. There are, however, distinct ranges of q^2 where μ_{exp} data lie almost perfectly on one of the branches provided by the rigorous calculation (on μ_1 for $q^2 < 3.5$, on μ_2 for $5.0 < q^2 < 6.7$ and on μ_3 for $8.0 < q^2 < 10.0$).

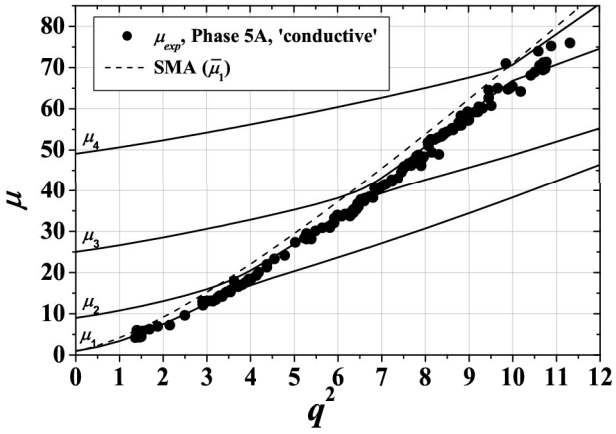

FIG. 6: Theoretical and measured values of the dimensionless decay rate μ of the director versus dimensionless q^2 for Phase 5A in the 'conductive' regime. Solid lines correspond to the four lowest $\mu_k(q^2)$ branches of the dispersion relation, the dashed line shows the expectation of the SMA ($\bar{\mu}_1(q^2)$). Solid circles are the data for μ_{exp} measured at sinusoidal excitation.

Figure 7 displays the measured decay rates together with the theoretical curves for the whole q range, including the 'dielectric' mode. The trend of the persistent switching of μ_{exp} to higher μ_k branches with increasing q^2 continues in the dielectric regime. This similarity is actually not surprising, although the electroconvecting state in the 'dielectric' regime is crucially different from that of the 'conductive' one (e.g. the director tilt follows the excitation frequency which can be nicely detected in the oscillating intensity of the diffraction fringes), the decay itself occurs under the same field-off condition in both cases.

These data indicate that the assumption of the final decay occurring with the slowest mode does not hold or at least cannot be justified with the spatio-temporal resolution facilitated by our experimental set-up. Surprisingly the slowest mode μ_1 is not reflected in the diffracted light intensity (except for small q^2). Instead the decay rate $\mu_k(q^2)$ with the eigenfunction $N_k(z)$ closest to $cos(z)$ (with small superimposed oscillations as shown in Fig. 3) dominates. Apparently this eigenfunction has the largest overlap with the initial director field and thus provides the largest weights A_i. With increasing q^2 this eigenfunction appears at higher indices k of the eigenvalues μ_k. As a result the system switches from one branch to the next.

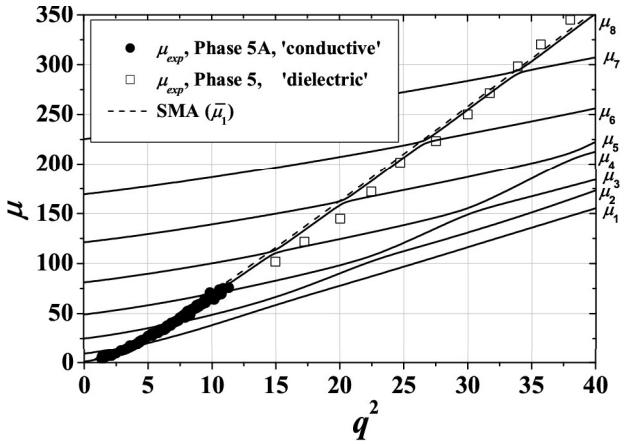

FIG. 7: Theoretical and measured values of the dimensionless decay rate μ of the director versus dimensionless q^2. Solid lines correspond to branches $\mu_k(q^2)$ of the dispersion relation, the dashed line shows the SMA result $\bar{\mu}_1(q^2)$. Solid circles and open squares are the data for μ_{exp} measured in the 'conductive' regime of Phase 5A and in the 'dielectric' regime of Phase 5 respectively.

For q^2 in the switching region the measured μ_{exp} falls in between the branches indicating the absence of a single dominating mode. Actually fitting the decay curves with a superposition of more exponentials reduces the mean square deviation slightly in those regions. Preliminary calculations which follow the general scheme presented at the end of Section II, show indeed that for $q^2 = 10$ (conductive regime, see Fig. 6) where $\mu \approx \mu_3$ the contribution of this mode to the fringe intensity I_1 is larger by a factor $30 - 50$ compared to the contribution of the modes μ_1 and μ_2.

V. CONCLUSIONS

A rigorous theoretical solution has been provided for the problem of the decay modes of periodic patterns in nematic liquid crystals. The proper handling of the boundary conditions has yielded a dispersion relation with a sequence of modes with different relaxation times in contrast to the single exponential decay predicted by the slowest SMA mode. The branches of the dispersion relation have been calculated for the nematic liquid crystal Phase 5/5A.

Laser diffraction at an oblique incidence has turned out to be an excellent tool to monitor the decay process experimentally. The decay rates have been measured in a wide wavenumber range. Several distinct q ranges have been found where the relaxation of the pattern is characterized by an exponential decay slightly slower than that given by the SMA, but coinciding with one of the calculated branches of the dispersion relation. That indicates that the generally multimode decay is usually dom-

inated by a single mode though somewhat different from that provided by the SMA. This trend holds for both the 'conductive' and the 'dielectric' regimes showing that the type of excitation has only a minor influence on the decay process. The detailed analysis of the impact of the initial conditions including a theoretical decomposition into modes is still under investigation.

Acknowledgments

Financial support by the Hungarian Research Grants No. OTKA-T031808, OTKA-T037336, OM00224/2001 and the EU Research Training Network PHYNECS is gratefully acknowledged.

[1] Á. Buka and L. Kramer Eds.,*Pattern Formation in Liquid Crystals*, (Springer-Verlag, New York, 1996).
[2] L. Kramer and W. Pesch, in *Pattern Formation in Liquid Crystals*, edited by Á. Buka and L. Kramer (Springer-Verlag, New York, 1996) pp. 221-255.
[3] A. Buka, B. Dressel, W. Otowski, K. Camara, T. Toth-Katona, L. Kramer, J. Lindau , G. Pelzl and W. Pesch, Phys. Rev. E **66**, 051713/1-8 (2002).
[4] A.Buka, B.Dressel, L.Kramer and W.Pesch, Phys.Rev.Lett. **93**, 044502 (2004)
[5] M. Treiber, and L. Kramer, Mol. Cryst. Liq. Cryst. **261**, 311 (1995).
[6] R. A. Rigopoulos, and H. M. Zenginoglou, Mol. Cryst. Liq. Cryst. **35**, 307 (1976).
[7] P. L. Papadopoulos, H. M. Zenginoglou, and J. A. Kosmopoulos, J. Appl. Phys. **86**, 3042 (1999).
[8] H. M. Zenginoglou, and J. A. Kosmopoulos, Appl. Opt. **28**, 3516 (1989).
[9] J. A. Kosmopoulos, and H. M. Zenginoglou, Appl. Opt. **26**, 1714 (1987).
[10] H. M. Zenginoglou, and J. A. Kosmopoulos, J. Opt. Soc. Am. A **14**, 669 (1997).
[11] T. John, U. Behn, and R. Stannarius, Eur. Phys. J. B **35**, 267 (2003).
[12] H. M. Zenginoglou, and J. A. Kosmopoulos, Appl. Opt. **27**, 3898 (1988).
[13] P. G. deGennes, *The Physics of Liquid Crystals*, (Clarendon Press, Oxford, 1974).
[14] S. Chandrasekhar, *Liquid Crystals*, (University Press, Cambridge, 1992).
[15] H. Pleiner and H. R. Brand, in *Pattern Formation in Liquid Crystals*, edited by Á. Buka and L. Kramer (Springer-Verlag, New York, 1996) pp. 15-67.
[16] M. Treiber, N. Éber, Á. Buka, and L. Kramer, J. Phys. II France **7**, 649 (1997).
[17] H. H. Graf, H. Kneppe and F. Schneider, Mol. Phys. **77**, 521 (1992).